Chemical and Process Engineering: New Frontiers, 2023, 44(3), e17
DOI: 10.24425/cpe.2023.146719

Utilization of cylindrical Cu/Fe galvanic cell as an effective method for the removal of humic acids

Bartosz Libecki, Tomasz Mikołajczyk*, Bogusław Pierożyński, Mateusz Kuczyński

University of Warmia and Mazury in Olsztyn, Faculty of Agriculture and Forestry, Department of Chemistry, Łódzki Square 4, 10-727 Olsztyn, Poland

*** Corresponding author:**
e-mail:
tomasz.mikolajczyk@uwm.edu.pl

Presented at 24th Polish Conference of Chemical and Process Engineering, 13–16 June 2023, Szczecin, Poland.

Article info:
Received: 7 April 2023
Revised: 27 June 2023
Accepted: 4 July 2023

Abstract
Humic substances (HS) are hydrophobic parts of dissolved organic matter, which are hard to degrade using biological processes. When exposed to disinfection processes, the HS present in wastewater could lead to the formation of disinfection by-products (DBPs), which are harmful and dangerous to health. Thus, a chemical coagulation process is commonly used for HS removal. This work used a cylindrical galvanic cell (CGC) with an iron anode and a copper cathode, where the dissolution of the anode served as an alternative source of metal ions for HS coagulation. The galvanic cell current for CGC stabilized at around 0.6 mA, and the voltage fluctuated, *ca.* 0.5 V for all solutions. The peaks observed on cyclic voltammograms could be associated only with oxidation and dissolution of iron; no other process was identified. After the process, the structures and molecular composition of the anode surface suggest the loss of Fe mass and the formation of iron oxides due to corrosion. The initial pH of the tested solution influenced the total Fe oncentration in the solution as well as colour and turbidity. The quantitative removal of HS by electrolysis and membrane filtration processes at initial $pH_i = 6.0$ yielded 72% and 90%, respectively, after 6 and 10 min. The mechanism of sorption on the flocs of hydroxides as a primary factor in HA removal was suggested.

Keywords
galvanic cell, iron anode, electrochemical coagulation, humic acids removal

1. INTRODUCTION

Humic substances (HS) are a heterogeneous group of compounds among which the soluble fraction – fulvic acids (FA) and humic acids (HA) are the main components of hydrophobic organic matter in total dissolved organic carbon (DOC) (Chanudet et al., 2006; Klučáková, 2018) present in water and sewage (Imai et al., 2002; Łomińska-Płatek and Anielak, 2019). The HS are complex long-chain polymers with hydrophobic polyphenolic skeleton and hydrophilic functional groups, making them acidic (Łomińska-Płatek and Anielak, 2019; Tatzber et al., 2007). The number of these groups in the acid structure, composition, and molecular weight is variable and depends on the source of origin (Asakawa et al., 2011; Klučáková, 2018). They are responsible for changing the physical properties such as pH and colour of water intended for domestic and economic purposes. HA show chelating properties and can accumulate heavy metals and transfer them from the environment to the waters (Benegas et al., 2003; Pastorelli et al., 1999). HS, known as the so-called Refractory Organic Substances (ROS), pose a potential health hazard due to generating disinfection by-products DBPs in water treatment processes (Hesse et al., 1999). The aromatic fraction of DOC measured at A_{254} nm is mainly responsible for forming DBPs (Golea et al., 2017).

Due to the high resistance to biochemical decomposition processes, physicochemical methods are used to remove DOC containing HS, usually combined into hybrid technologies consisting of coagulation/flocculation, adsorption, oxidation and filtration processes (Sillanpää and Matilainen, 2015). Due to the limits of membrane filter technology (Alresheedi et al., 2019), the content of HA and FA should be initially reduced with effective physicochemical methods. Coagulation using aluminium and iron salts is commonly used to remove HA, as it has good efficiency and moderate costs, but it requires an advanced technical infrastructure (Heiderscheidt et al., 2013; Ratnaweera and Fettig, 2015). A significant disadvantage of this method is secondary water pollution after the introduction of coagulants, which is manifested by a decrease in pH and an increase in salinity (Jiang, 2015).

Similarly, to coagulation with salts, metal ions dissolved during electrocoagulation (EC) and were capable of binding DOC molecules. Thanks to the electrochemical dissolution of Al, Fe and Zn anodes combined with microfiltration could obtain the removal at a level of 75% of DOC and 89% of UV A_{254} (Dubrawski et al., 2013). Electricity consumption for the EC methods that used iron electrodes depended on the pH and conductivity of the solution and ranged from 0.7 to 1.7 kWh/g HA (Bazrafshan et al., 2012). In other bog water treatment studies, the EC achieved HS removal efficiency of 62-75% with an energy consumption of 0.35–0.70 kWh/m^3 (Kuokkanen et al., 2015).

The introduction of metal ions into the solution often occurs spontaneously due to corrosive processes. For example, corrosion problems appear in steel installations, such as pipelines, in contact with the aquatic environment (Sean

Brossia, 2014). Corrosion takes place on the steel surface due to the heterogeneity of the structure, ion interactions and changes in the concentration of the electrolyte at the electrode surface (Ji et al., 2013). As a result, there is a potential difference at the surface, causing the formation of macro or micro galvanic cells. When two different metals are immersed in an electrolyte, they form a cell according to an electrochemical series.

The anodic dissolution phenomenon, characteristic of a galvanic cell, is observed in places with a lower potential on the steel surface (Ji et al., 2013; Zhu et al., 2018):

- Anodic oxidation:

$$Fe^0 - 2e^- \rightarrow Fe^{2+} \quad (1)$$

where, E $(Fe^{2+}/Fe) \approx -0.44$ V

- Cathodic reduction:

$$2H_2O + O_2 + 4e^- \rightarrow 4OH^- \quad (2)$$

where, E $(O_2/OH^-) \approx +0.40$ V.

The lower potential metal becomes the anode. After the electrodes are shorted, a corrosive current appears, the density of which increases significantly in the presence of oxygen (Smallman and Bishop, 1999). These naturally occurring processes have been employed for wastewater treatment as an iron-copper galvanic system (Libecki and Pierożyński, 2019). It was used for purification of industrial effluents (Alcalá-Delgado et al., 2018), dyes (Kuczyński et al., 2021), or phenol (Pierozynski and Piotrowska, 2018). The galvanic cell (GC) as a water treatment could be considered clean, cost-effective and easy to apply, which supports the Sustainable Development Goals (SDG 6) (Martínez-Huitle et al., 2021). Additionally, it can reach removal efficiency at the level of the Fenton reaction (Alcalá-Delgado et al., 2018). The galvanic cell process with the chemical oxidation of H_2O_2 allows the removal of the refractory hydrophobic fraction from the landfill leachates and enables their further purification using biological methods (Castillo-Suárez et al., 2019). However, there is a lack of articles on the process removal of humic acids by means of macro galvanic cells.

This paper presents a method of purifying water containing humic acids using cylindrical galvanic Cu/Fe cell (CGC). The research aimed to check the efficiency of treatment and CGC operating parameters at low conductivity – 500 µS/cm of the solution (the limit for drinking water 2500 µS/cm) (Council Directive 98/83/EC).

2. EXPERIMENTAL

2.1. Solutions of humic acids (HA)

A solution of humic acids (Sigma-Aldrich) was used for the experiments. The solution was prepared from a dry sample of 500 mg of humic acids, diluted in 100 mL of 0.5 M Na_2CO_3 solution. The solution was allowed to settle for 48 h and then filtered through a 0.45 µm membrane filter (PALL Co. cellulose acetate). The test solution was prepared by diluting 5 mL of HA alkaline solution in 1 L of H_2O. The tests were carried out in solutions at pH = 7.6, and pH = 6.0 (samples 1 and 2, correspondingly). 1 M hydrochloric acid was used to adjust the pH. The reagents used were of analytical purity, and the deionized water was 2.5 µS/cm ±0.5.

Table 1. Characteristic of the model HA solutions.

Parameter	Solution 1	Solution 2
pH	7.63 ± 0.05	5.99 ± 0.04
Conductivity [µS/cm]	502 ± 1	531 ± 16
Colour [PtCo]	413 ± 14	342 ± 2.5
Turbidity [NTU]	0.28 ± 0.03	0.38 ± 0.03
A_{254} [cm^{-1}]	0.747 ± 0.014	0.746 ± 0.029
DOC [mg/L]	7.81 ± 0.24	7.81 ± 0.24

2.2. Experimental techniques

The tests were carried out with the use of a CGC (Fig. 1), where the inner electrode-anode was made of unalloyed carbon steel with an active surface area of 18 cm^2, and the outer electrode cathode was made of copper. The space between the electrodes was 4.5 mm. Before the experiment, the electrodes were cleaned by immersion in a 6% HCl solution. Additionally, the anode before immersion in HCl solution was polished using grinding paper of 2000 grade.

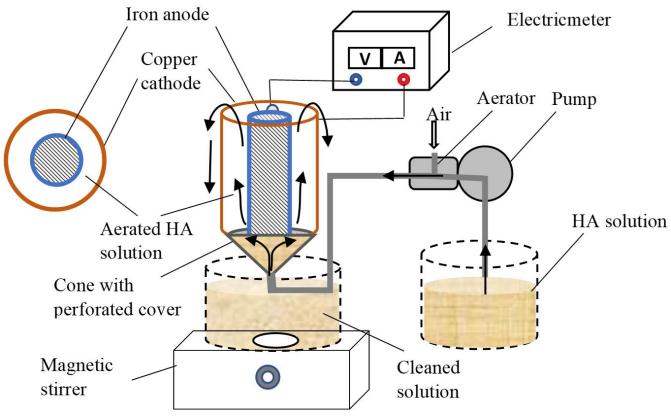

Figure 1. Scheme of the laboratory scale purification system with the cylindrical galvanic cell (CGC).

For each measurement, the humic acid (HA) solution was individually pumped into the cell from the tank using a pipe. An air pump supplied a steady stream of air (3 mL/min) directly into the flowing solution through a splitter to ensure constant airflow. The contact time (CT) between the solution and the electrode surface was carefully regulated and adjusted for

each measurement, ranging from 1 to 11 minutes. The peristaltic pump rotation was used to control the duration of contact time.

Following the specific hold time for each measurement, the solution was directed into a separate reservoir positioned on a magnetic stirrer and mixed at a speed of *ca.* 200 rpm. After pumping approximately 50 mL of the solution, it was left undisturbed for 1 hour to allow sedimentation to occur. The process was repeated for different contact times to evaluate the effectiveness of the treatment technique at varying durations.

2.3. Electrochemical measurements

Electrochemical measurements were carried out during the operation of the cell. The open cell potential was measured in the experiment's first phase until its value stabilized. After that, the circuit was closed, and the current was measured while the cell was operating. Finally, the voltage value was recorded after the set time. The measurement was repeated three times.

The electrochemical characterization of Fe dissolution was done through cyclic voltammetry with a Multi-Autolab potentiostat/galvanostat system (AUTM204). The cyclic voltammetry experiments were carried out at a sweep-rate of 50 mV/s over the working electrode potential ranges of -1.1- 2.0 V vs. SCE (saturated calomel electrode). The instruments were controlled by Nova 2.1 software for Windows (Metrohm Autolab B.V., Opacz-Kolonia, Poland). Also, all data analysis was performed with the software mentioned above. The cell was immersed in a pH-regulated solution with and without HA and aerated.

2.4. Physicochemical measurements

Physicochemical analyses were performed in the supernatant solution, i.e., pH, conductivity (Elmetron), apparent colour (mg PtCo/ L) (HACH method 8025), turbidity (NTU) (TIR 200 VWR) and DOC (TOC 5000 analyzer Shimadzu). The UV absorbancy A_{254} (UV-1600PC VWR) analysed after 0.45 µm membrane filtration.

Fe_{tot}. marked by the thiocyanate method with sludge mineralization. In order to determine the concentration of dissolved Fe, samples of the solution were mineralized at 100 °C for approx. 5 min with $K_2S_2O_8$ under strongly acidic conditions with HCl. After cooling, NH_4SCN was added and analysed calorimetrically at $\lambda = 480$ nm using the Abs/Fe concentration (mg/L) standard curve (the quantification limit of this method was on the level of 0.1 mg Fe^{3+}/L).

Spectroscopic characterization and elemental composition of the anode surface were performed by means of Quanta FEG 250 Scanning Electron Microscope (SEM), equipped with an Energy Dispersive X-ray Spectroscopy (EDX) (Bruker XFlash 5010). EDX tests were carried out at an acceleration voltage of 12 keV.

3. RESULTS AND DISCUSSION

3.1. Electrical and chemical effect of CGC working in the solutions

During the experiment, the operation of the cell was monitored by measuring the values of the open circuit potential and the working current after the anode surface's contact time (CT) with the HA solution (Fig. 2). The cell voltage during the tests fluctuated around 0.5 V for both solutions and was slightly higher for solution 2 ($pH_i = 6.0$) than for solution 1 ($pH_i = 7.6$).

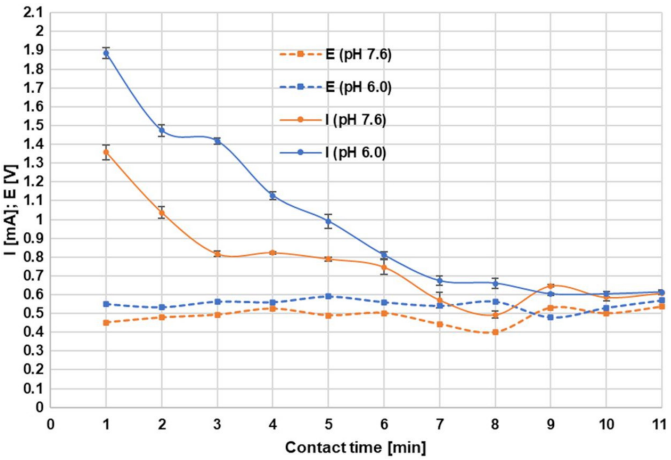

Figure 2. Changes in potential and current in a CGC depending on the operating time.

Additionally, contact time had a direct correlation with the working current of the cell, with higher values observed for faster solution flow (shorter CT). This phenomenon can be attributed to the accumulation of corrosion products within the volume of the solution. When the solution flows faster, there is limited time for the corrosion products to settle or deposit on the working electrode's surface.

In contrast, when the solution flow is slower, the accumulation of corrosion products becomes more pronounced. These products have the potential to deposit and form a layer on the working electrode's surface, thereby blocking its active area; thus, decreasing the operating current. The corrosion rate is usually controlled by the rate of oxygen diffusion to the surface of the steel. Aeration mechanically unblocks the anode surface, and the process continues until the corrosion equilibrium is established (Huet et al., 2007).

3.2. Cyclic voltammetry (CV) characterization of the surface oxidation process

The CV characterization (Fig. 3) of the Fe anode surface oxidation process in solutions 1 (pH = 7.6) and 2 (pH = 6.0) and in buffer solution (pH = 8.4) without HA was carried-out over the potential span –1.1 ÷ 2.0 V/SCE with a scan rate of 50 mV/s (only second sweeps are presented). Two irreversible anodic peaks could be observed for the cyclic voltammogram recorded in the absence of the HA: a low potential centred at about –0.44 V and another one positioned at ca. –0.05 V vs SCE. Thus, the former peak is related to the process of Fe(II) formation, whereas the latter one could be assigned to its further oxidation to form $Fe(OH)_3$ surface layers (Cabrera-Sierra et al., 2002; El-Naggar, 2004).

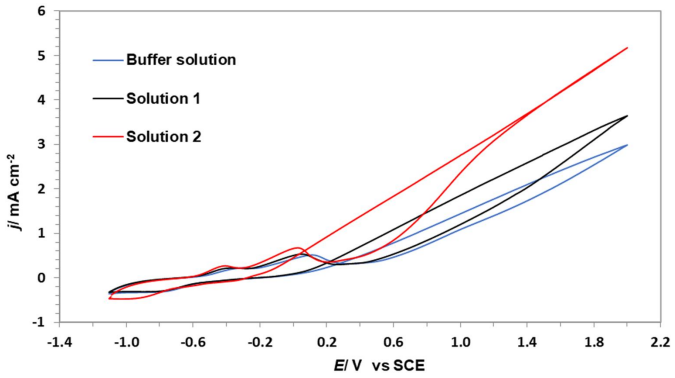

Figure 3. Cyclic voltammetry behaviour of the CGC in three different solutions, recorded at a sweep-rate of 50 mV/s and 293 K (second cycle).

Then, introducing HA into the buffer solution did not cause significant differences in the CV profiles. The only noticeable changes were an increase in current density and a minor potential shift of the peaks. However, they could be associated with lower pH values of solutions 1 and 2 compared to the buffer solution.

3.3. SEM/EDX Characterization of CGC

Figures 4a and 4b show an SEM micrograph of the Fe anode surface before and after the electrolysis process. Table 2 shows the SEM/EDX results for the percentage of individual components on the anode surface before and after the electrolysis. After the process, the anode has a damaged surface with visible structures of incrustation and pitting character compared to the surface before electrolysis. The effect of surface oxidation is evidenced by an increase in oxygen content by over 21% after the process.

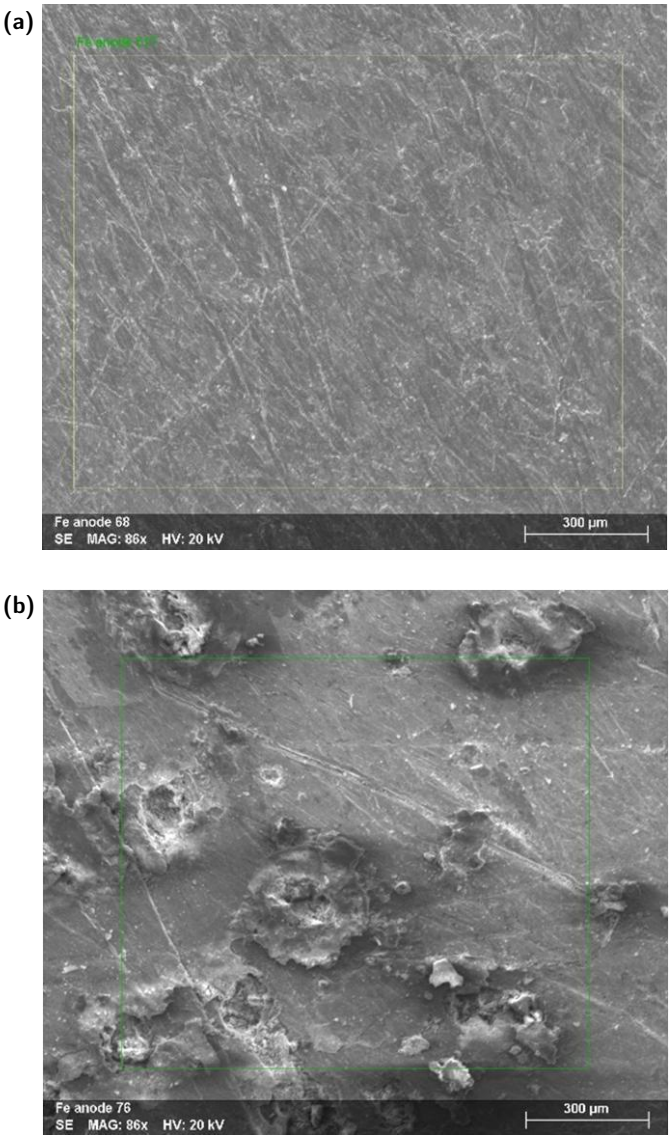

Figure 4. Image of the anode surface: (a) before, (b) after electrolysis.

The impact of the entire surface of the electrodes in the macrogalvanic cell, the anode corrosion process is rapid, manifested by an increase in pH. Fe^{2+} ions in a further step hy-

Table 2. The elementary composition of the surface anode layer before and after electrolysis.

Element	Iron	Carbon	Oxygen	Sodium	Chlorine
Before electrolysis					
Mass Norm. [%]	90.75 ± 2.7	6.4 ± 2.1	2.29 ± 0.42	0.76 ± 0.02	0
After electrolysis					
Mass Norm. [%]	67.85 ± 2.7	6.01 ± 2.1	24.0 ± 0.42	3.25 ± 0.02	0.45 ± 0.38

drolyse to form soluble hydroxides (Xiao et al., 2008):

$$Fe^{2+} + 2OH^- \rightarrow Fe(OH)_2 \quad (3)$$

$$4Fe^{2+} + O_2 + 2H_2O \rightarrow 4Fe^{3+} + 4OH^- \quad (4)$$

The phenomenon of oxidation of the electrode surface with rust products is generally known. Xiao et al. (2008) showed that the corrosion products of carbon steel were mainly γ-FeOOH, γ-Fe_2O_3, and a small amount of α-Fe_2O_3 reddish brown rust maghemite (γ-Fe_20_3) from lepidocrocite (γ-FeOOH):

$$2Fe(OH)_2 + \frac{1}{2}O_2 \rightarrow 2FeOOH + H_2O \quad (5)$$

$$2FeOOH \rightarrow Fe_2O_3 + H_2O \quad (6)$$

Additionally, chlorides detected on the anode surface come from the solution where they were present at 2 and 4 mmol after adjusting the pH to pH 7.6 and 6.0, respectively. By accumulating at the surface, chlorides can initiate pitting corrosion (Ji et al., 2013; Luo et al., 2017). Furthermore, with chlorine ions present, the following chemical reaction with Fe takes place, which has a catalytical effect (Xiao et al., 2021):

$$4Fe^{2+} + 8Cl^- \rightarrow 4FeCl_2 + 8OH^- + O_2 \rightarrow 4FeOOH + 8Cl^- + 2H_2O \quad (7)$$

As a result, new anode sites are activated, and the dissolution process escalates. On the other hand, in the presence of NOM, coordination processes take place on the surface of the steel, which can reduce the corrosion rate of the iron (Broo et al., 1999).

3.4. Impact on solution parameters

The influence of contact time (solution flow rate) shows noticeable differences between solutions 1 and 2, starting with a CT of 6 minutes, by the individual parameter values obtained through implementing the CGC, as illustrated in Figures 5 through 8. During the operation of the cell, evident changes in initial pH_i to final pH_f were noted – with increasing Fe discharge from the anode to the solution 1 and 2 (Fig. 5 and Fig. 6). The extension of contact time caused the increased solutions' pH to $pH_f = 8.4$ and $pH_f = 6.8$ for solutions 1 and 2 respectively. Similarly, the amount of dissolved iron in the solution increased with longer CTs reaching a concentration of 24 mg/L in solution 1. However, in the case of solution 2, lower iron values were reported compared to solution 1, with a maximum concentration observed at a contact time of 9 minutes (approximately 19 mg Fe/L).

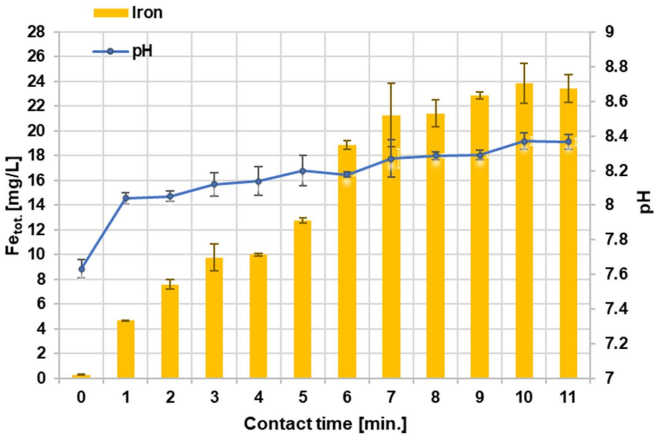

Figure 5. The pH and iron concentration values in solutions at $pH_i = 7.6$ after the contact time.

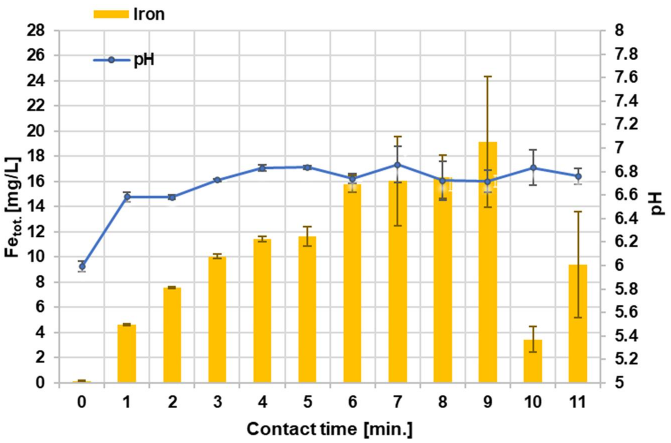

Figure 6. The pH and iron concentration values in solutions at $pH_i = 6.0$ after the contact time.

The lower iron concentrations at the lowered pH in solution 2 should rather be associated with the hydrolysis of dissolving iron and the extenuation of the dissociation of the humic molecules. Cationic hydrolysis products are strongly adsorbed on negative particles of HA; thus, destabilization occurs. It seems that lowering the pH_i of the solution to 6.0 enables the aggregation to proceed in the minimum contact time of 6 min. Subsequent flocculation leads to the sedimentation of parts of the flocs and decreases iron concentration in the solution (Duan and Gregory, 2003).

In the case of the colour parameter (Fig. 7), a steady increase was observed with longer contact times up to CT of 10 minutes in solution 1. Still, in solution 2, the increase was observed only till CT of 6 min and remained at a level of 950 mg PtCo/L for all CTs till 9 min. Then, for CT of 10 min, there was a significant decrease in the colour parameter value to *c.a.* 126 mg PtCo/L. At the same CT, the colour parameter of solution 1 was an order of magnitude higher (1350 PtCo/L).

An almost identical pattern was observed in the turbidity parameter for both solutions (Fig. 8). Particle growth due to aggregation processes, with larger particles exhibiting a greater interfering effect with the path of the light beam, causing scattering, reflecting, and blocking effects. This characteristic can be utilized to accurately determine the threshold dose of online coagulation (Libecki et al., 2020). However,

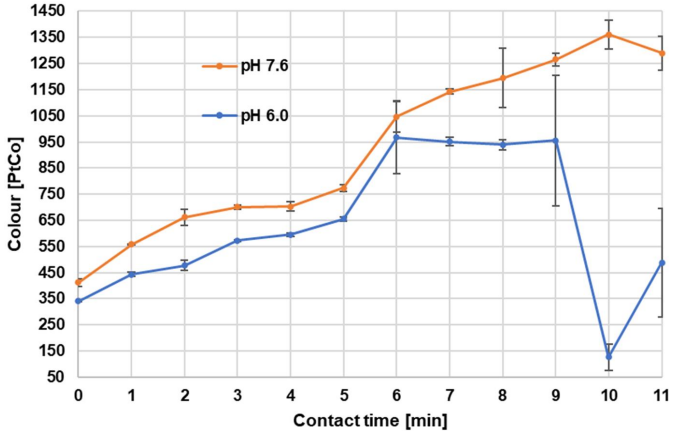

Figure 7. The changes in the colour of the solution depending on pH_i and contact time.

in solution 2, the coagulation threshold of iron concentration was reached at a CT of 9 minutes. Thus, longer CTs led to precipitation and subsequent reduction in turbidity. All the above suggests that iron concentration and pH significantly determine the solution's colour and turbidity.

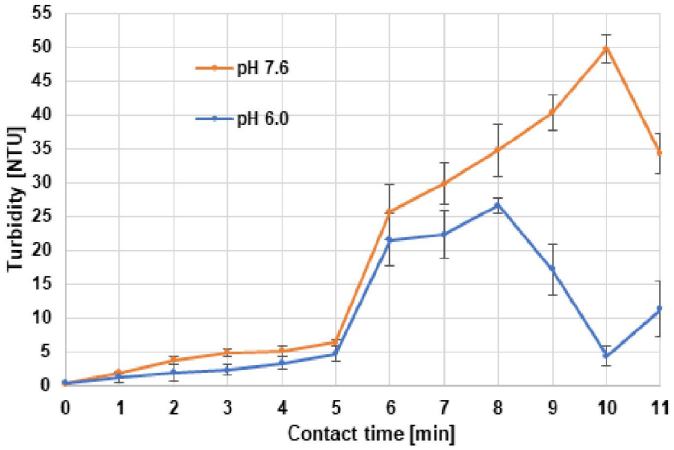

Figure 8. The changes of turbidity of the solution depending on pH_i and contact time.

From the analysis of Fig. 9a, a strong relationship ($R^2 = 0.98$) between the solution colour and iron concentration was observed in the test samples in solution 1. Also, in solution 2, a good relationship was still present; however, it appeared to be slightly weaker ($R^2 = 0.82$). No precipitate was observed in the solution with pH 7.6, indicating that the hydrolysis products were likely bound by the dissolved humic acid (HA) molecules. As a result, some of the iron ions existed in the form of dissolved organic complexes. Conversely, in the case of pH 6.0, a portion of the iron remained dissolved in the solution while a significant amount underwent precipitation, as mentioned earlier.

In the presence of oxygen, oxidation occurs, leading to the formation of Fe(III) hydroxide species. These species exist as aqua complexes, $[Fe(OH)_3(H_2O)_x)]$, with their charge depen-

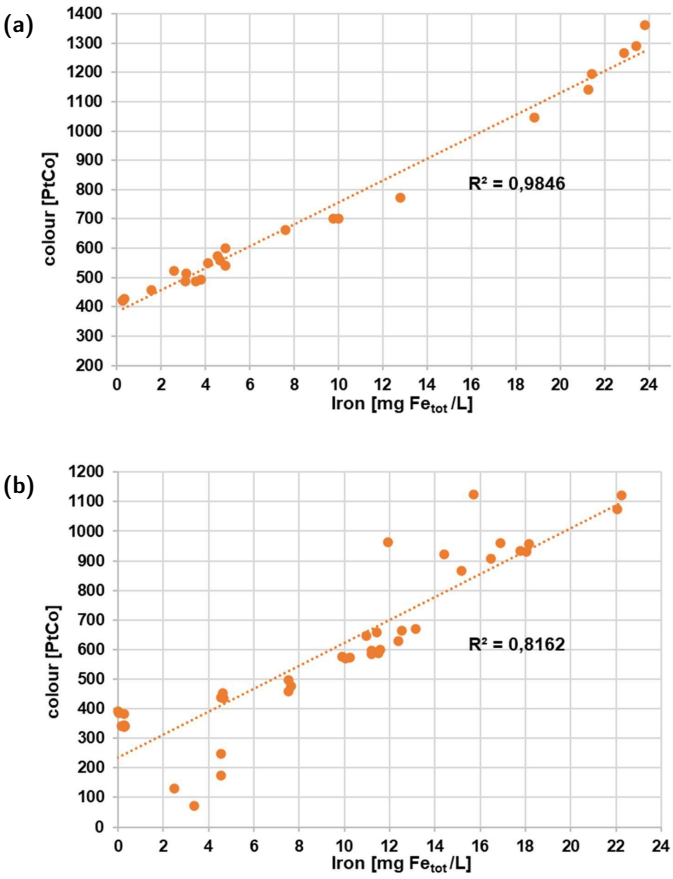

Figure 9. The relationship between the colour of the solution and the iron concentration after CGC treatment can be observed at two different pH levels: a) $pH_i = 7.6$ and b) $pH_i = 6.0$.

dent on the pH of the solution. It is known that these Fe hydrolysis products can interact with the aqueous organic matter, including humic acids present in the solution (Kislenko and Oliynyk, 2004). The presence of HS-associated Fe in aqueous solutions of chromophoric organic matter (such as fulvic and humic acids) results in a linear increase in light absorption at 410 nm with increasing concentration (Xiao et al., 2013). This phenomenon is attributed to the ability of humic acids to form chelates through functional groups present in their molecular structure, particularly aromatic structures from phenolic, carboxylic, and nitrogen groups (Pastorelli et al., 1999). The complexation of metals is influenced by the degree of deprotonation of molecules at a specific pH, the pK of the ligands, and the availability of Fe ions (Iffat et al., 2005).

Figure 10 presents the graph depicting the change in UV absorbance at 254 nm following CGC purification and membrane filtration at pH 7.6 and 6.0. The graph demonstrates over 72% and 90% purification efficiencies at CT of 6 and 10 minutes, respectively. Coagulation occurred, leading to sediment formation in trials conducted with CTs of 10 and 11 minutes.

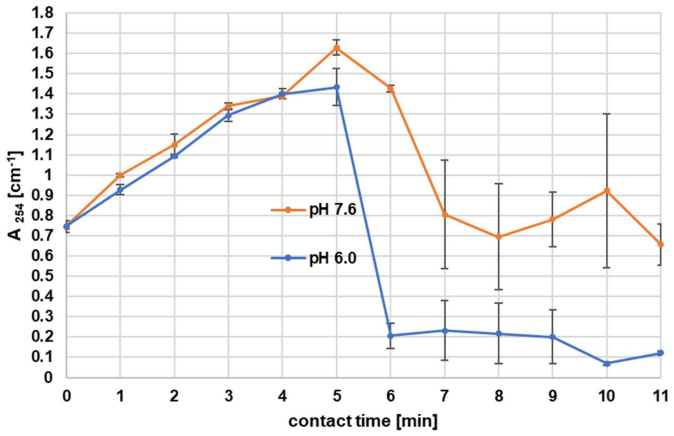

Figure 10. The changes of UV lights absorption at 254 nm of the filtered solution depending on pH_i and contact time.

At pH 7.6, it was noticed that the value of A_{254} also decreased as the CT exceeded 6 minutes. However, the actual A_{254} values obtained after post-treatment trials for CTs ranging from 6 to 11 minutes remained similar to the initial value. This phenomenon can be attributed to the inadequate aggregation of particles in solution 1, which impeded coagulation and resulted in the presence of small coloured particles, that the filtration membrane could not effectively capture. As a consequence, the assessment of efficient removal of humic acid (HA) from the solution was hindered.

Traditional chemical coagulation involves the addition of aluminium and iron salts to water in order to promote coagulation. Using this method, it is possible to achieve a 70% removal of DOC with the predominance of a hydrophobic DOC fraction, as measured absorbance at a wavelength of 254 nm (A_{254}) (Krupińska, 2023). In the treatment of surface waters, the aluminium coagulants ($Al_2(SO_4)_3$, PACl) and $FeCl_3$ demonstrates maximum effestiveness by removing 71–74% and 85% of UV_{254} respectively (Wang et al., 2013). These findings can be compared to other studies on the electrochemical purification of humic acid (HA). Ulu et al. (2014) electrochemically purified synthetic water prepared with 50 ppm Aldrich HA with a conductivity of 300 µS/cm after filtration with pore size 0.45 µm, obtained an 87% reduction of DOC using an iron electrode and 3 mA/cm^2 at pH_i = 4.0. Bazrafshan et al. (2012) showed that with an increase in conductivity from 1–3 mS/cm, the efficiency of electrocoagulation with iron electrodes increases by approx. 15% obtaining 92.7% HA removal at pH_i = 5. Lowering the pH increases the efficiency of the process by increasing the zeta potential, which determines floc formation by neutralizing the charge; on the other hand, an increase in the conductivity of the solution facilitates the compression of the double layer in colloid surfaces (Ulu et al., 2014). The studies of Jiménez et al. (2012) prove that the type of hydrolysed particles produced in an electrolytic cell depends on the pH, and in the case of iron, they form amorphous hydroxides with a positive charge in a wide range of pH 2–9. Hydrolysis products are involved in neutralizing the negatively charged dissolved HA particles. At the pH range of 4.0–6.0, the dominant form of iron (III) is $Fe(OH)_2^+$ species (Oriekhova and Stoll, 2014) which, thanks to its positive charge, allows better aggregation of flocs. Additionally, in an acidic environment, HA particles have lower ionisation. The above phenomena are responsible for improved aggregation and destabilisation of HA at a pH value of 6.0. In the further course of the process, destabilized particles combine to form large structures with a well-developed sorption surface, causing the so-called sweep flocculation (Ghernaout and Ghernaout, 2012). Ferric hydroxides show good sorption properties towards humic acids. This process is probably chemisorption in nature and can be described as a Langmuir isotherm model (Yousefi et al., 2019).

4. CONCLUSIONS

This paper presents a CGC galvanic cell operating in a HA solution. The cell consistently maintained a stable voltage of approximately 0.5 V at both pH levels. The working current decreased with longer contact times, but with CTs, higher than 6 minutes stabilized at a value of *ca.* 0.6 mA, regardless of pH. The cyclic voltammetry measurements showed that no oxidation of HA occurred during the electrocoagulation process. Thus, there is no indication of possible DBP generation through this process. After the process, the anode surface structures and molecular composition analysis indicated the intense course of pitting corrosion with Fe dissolution and the formation of iron oxides. The cell operation caused the alkalization of the solution by approx. 0.8 pH. Considerable colour increase in relation to the Fe concentration was observed, which means that a large proportion of the iron remained in the solution bound to the HA. An increase in turbidity for the CTs longer than 6 min and a sharp drop for the CT of 10 min indicate aggregation and precipitation, respectively. In the tests of the cell at CT = 10 min for pH_i = 7.6, the content of Fe came to 23.8 mg/L, while at pH_i = 6.0, the iron content was found to be 3.5 mg/L. The quantitative ratio Fe/ HA is required for optimal coagulation ≈ 1. On the other hand, after filtration through filters with a pore size of 0.45 mm, a 72% reduction of A_{254} can be obtained for CT of 6 min and over 90% for CT of 10 min.

The results indicate the possibility of including CGC in the upstream stage of purification systems for ROS removal. This method may be an effective alternative solution for water purifying from hydrophobic organic matter (A_{254}). Compared to the metal salt coagulants, the CGC method does not cause significant pH changes or increase water salinity; although, it can contribute to secondary water pollution by increasing Fe residue.

Further research is needed to determine the suitability of the cell for the purification of natural water. The efficiency of

the cell may vary depending on the origin of natural water and may change during the operation of the cell as a result of other factors. Nevertheless, a galvanic cell which needs a minimal dose of reagents for pH correction and has a simple and compact design is a perfect example of low emission water treatment technology.

AKNOWLEDGMENTS

The results in this paper were obtained as part of a comprehensive study financed by the University of Warmia and Mazury in Olsztyn, Faculty of Agriculture and Forestry, Department of Chemistry (grant no. 30.610.001-110).

SYMBOLS

A_{254}	absorbance in UV region at 254 nm optical length, cm^{-1}
CGC	cylindrical galvanic cell
CT	contact time, min.
CV	cyclic voltammetry
DBPs	disinfection by-products
DOC	dissolved organic carbon, mg C/L
E	potential, V
EC	electrocoagulation
EDX	energy dispersive X-ray spectroscopy
FA	fulvic acids
GC	galvanic cell
HA	humic acids
HS	humic substances
I	current, mA
j	current-density, mA/cm^2
NOM	natural organic matter
ROS	Refractory Organic Substances
SCE	saturated calomel electrode
SEM	Scanning Electron Microscope

REFERENCES

Alcalá-Delgado A.G., Lugo-Lugo V., Linares-Hernández I., Martínez-Miranda V., Fuentes-Rivas R.M., Ureña-Nuñez F., 2018. Industrial wastewater treated by galvanic, galvanic Fenton, and hydrogen peroxide systems. *J. Water Process Eng.*, 22, 1–12. DOI: 10.1016/j.jwpe.2018.01.001.

Alresheedi M.T., Barbeau B., Basu O.D., 2019. Comparisons of NOM fouling and cleaning of ceramic and polymeric membranes during water treatment. *Sep. Purif. Technol.*, 209, 452–460. DOI: 10.1016/j.seppur.2018.07.070.

Asakawa D., Iimura Y., Kiyota T., Yanagi Y., Fujitake N., 2011. Molecular size fractionation of soil humic acids using preparative high performance size-exclusion chromatography. *J. Chromatogr. A*, 1218, 6448–6453. DOI: 10.1016/j.chroma.2011.07.030.

Bazrafshan E., Biglari H., Mahvi A.H., 2012. Humic acid removal from aqueous environments by electrocoagulation process using iron electrodes. *J. Chem.*, 9, 2453–2461. DOI: 10.1155/2012/876739.

Benegas J.C., Porasso R.D., van den Hoop M.A.G.T., 2003. Proton–metal exchange processes in synthetic and natural polyelectrolyte solution systems. *Colloids Surf., A*, 224, 107–117. DOI: 10.1016/S0927-7757(03)00327-3.

Broo A.E., Berghult B., Hedberg T., 1999. Drinking water distribution – the effect of natural organic matter (NOM) on the corrosion of iron and copper. *Water Sci. Technol.*, 40, 17–24. DOI: 10.2166/wst.1999.0432.

Cabrera-Sierra R., Sosa E., Oropeza M.T., González I., 2002. Electrochemical study on carbon steel corrosion process in alkaline sour media. *Electrochim. Acta*, 47, 2149–2158. DOI: 10.1016/S0013-4686(02)00090-7.

Castillo-Suárez L.A., Lugo-Lugo V., Linares-Hernández I., Martínez-Miranda V., Esparza-Soto M., Mier-Quiroga M.Á., 2019. Biodegradability index enhancement of landfill leachates using a Solar Galvanic-Fenton and Galvanic-Fenton system coupled to an anaerobic–aerobic bioreactor. *Sol. Energy*, 188, 989–1001. DOI: 0.1016/j.solener.2019.07.010.

Chanudet V., Filella M., Quentel F., 2006. Application of a simple voltammetric method to the determination of refractory organic substances in freshwaters. *Anal. Chim. Acta*, 569, 244–249. DOI: 10.1016/j.aca.2006.03.097.

Council Directive 98/83/EC of 3 November 1998 on the quality of water intended for human consumption. *OJ*, L 330, 32–54, 05.12.1998. Available at: https://eur-lex.europa.eu/eli/dir/1998/83/oj.

Duan J., Gregory J., 2003. Coagulation by hydrolysing metal salts. *Adv. Colloid Interface Sci.*, 100–102, 475–502. DOI: 10.1016/S0001-8686(02)00067-2.

Dubrawski K.L., Fauvel M., Mohseni M., 2013. Metal type and natural organic matter source for direct filtration electrocoagulation of drinking water. *J. Hazard. Mater.*, 244–245, 135–141. DOI: 10.1016/j.jhazmat.2012.11.027.

El-Naggar M.M., 2004. Cyclic voltammetric studies of carbon steel in deaerated $NaHCO_3$ solution. *J. Appl. Electrochem.*, 34, 911–918. DOI: 10.1023/B:JACH.0000040448.93720.2d.

Ghernaout D., Ghernaout B., 2012. Sweep flocculation as a second form of charge neutralisation—a review. *Desalination Water Treat.*, 44, 15–28. DOI: 10.1080/19443994.2012.691699.

Golea D.M., Upton A., Jarvis P., Moore G., Sutherland S., Parsons S.A., Judd S.J., 2017. THM and HAA formation from NOM in raw and treated surface waters. *Water Res.*, 112, 226–235. DOI: 10.1016/j.watres.2017.01.051.

Heiderscheidt E., Saukkoriipi J., Ronkanen A.-K., Kløve B., 2013. Optimisation of chemical purification conditions for direct application of solid metal salt coagulants: Treatment of peatland-derived diffuse runoff. *J. Environ. Sci.*, 25, 659–669. DOI: 10.1016/S1001-0742(12)60111-9.

Hesse S., Kleiser G., Frimmel F.H., 1999. Characterization of refractory organic substances (ROS) in water treatment. *Water Sci. Technol.*, 40, 1–7. DOI: 10.2166/wst.1999.0429.

Huet B., L'hostis V., Santarini G., Feron D., Idrissi H., 2007. Steel corrosion in concrete: Determinist modeling of cathodic reaction as a function of water saturation degree. *Corros. Sci.*, 49, 1918–1932. DOI: 10.1016/j.corsci.2006.10.005.

Iffat A.T., Maqsood Z.T., Fatima N., 2005. Study of complex formation of Fe(III) with tannic acid. *J. Chem. Soc. Pak.*, 27, 174–177.

Imai A., Fukushima T., Matsushige K., Kim Y.-H., Choi K., 2002. Characterization of dissolved organic matter in effluents from wastewater treatment plants. *Water Res.*, 36, 859–870. DOI: 10.1016/S0043-1354(01)00283-4.

Ji Y., Zhao W., Zhou M., Ma H., Zeng P., 2013. Corrosion current distribution of macrocell and microcell of steel bar in concrete exposed to chloride environments. *Constr. Build. Mater.*, 47, 104–110. DOI: 10.1016/j.conbuildmat.2013.05.003.

Jiang J.-Q., 2015. The role of coagulation in water treatment. *Curr. Opin. Chem. Eng.*, 8, 36–44. DOI: 10.1016/j.coche.2015.01.008.

Jiménez C., Sáez C., Martínez F., Cañizares P., Rodrigo M.A., 2012. Electrochemical dosing of iron and aluminum in continuous processes: A key step to explain electro-coagulation processes. *Sep. Purif. Technol.*, 98, 102–108. DOI: 10.1016/j.seppur.2012.07.005.

Kislenko V.N., Oliynyk L.P., 2004. Treatment of humic acids with ferric, aluminum, and chromium ions in water. *J. Colloid Interface Sci.*, 269, 388–393. DOI: 10.1016/j.jcis.2003.07.040.

Klučáková M., 2018. Size and charge evaluation of standard humic and fulvic acids as crucial factors to determine their environmental behavior and impact. *Front. Chem.*, 6, 235. DOI: 10.3389/fchem.2018.00235.

Krupińska I., 2023. Suitability of highly polymerised polyaluminium chlorides (PACls) in the treatment of mixture of groundwater and surface water. *Molecules*, 28, 468. DOI: 10.3390/molecules28020468.

Kuczyński M., Łuba M., Mikołajczyk T., Pierożyński B., Jasiecka-Mikołajczyk A., Smoczyński L., Sołowiej P., Wojtacha P., 2021. Electrodegradation of acid mixture dye through the employment of Cu/Fe macro-corrosion galvanic cell in Na_2SO_4 synthetic wastewater. *Molecules*, 26, 4580. DOI: 10.3390/molecules26154580.

Kuokkanen V., Kuokkanen T., Rämö J., Lassi U., 2015. Electrocoagulation treatment of peat bog drainage water containing humic substances. *Water Res.*, 79, 79–87. DOI: 10.1016/j.watres.2015.04.029.

Libecki B., Kalinowski S., Wardzyńska R., Bęś A., 2020. Using an angular detection photometer (ADP) in analyzing the humic acids coagulation process. *J. Water Process Eng.*, 37, 101507. DOI: 10.1016/j.jwpe.2020.101507.

Libecki B., Pierożyński B., 2019. *Auto electro coagulating device*. PL231445B1.

Łomińska-Płatek D., Anielak A.M., 2019. Characteristic of fulvic acids extracted from the wastewater by different methods. *Annual Set The Environment Protection*, 21(1), 184–200.

Luo H., Su H., Dong C., Li X., 2017. Passivation and electrochemical behavior of 316L stainless steel in chlorinated simulated concrete pore solution. *Appl. Surf. Sci.*, 400, 38–48. DOI: 10.1016/j.apsusc.2016.12.180.

Martínez-Huitle C.A., Sirés I., Rodrigo M.A., 2021. Editorial overview: Electrochemical technologies for wastewater treatment with a bright future in the forthcoming years to benefit of our society. *Curr. Opin. Electrochem.*, 30, 100905. DOI: 10.1016/j.coelec.2021.100905.

Oriekhova O., Stoll S., 2014. Investigation of $FeCl_3$ induced coagulation processes using electrophoretic measurement, nanoparticle tracking analysis and dynamic light scattering: Importance of pH and colloid surface charge. *Colloids Surf., A*, 461, 212–219. DOI: 10.1016/j.colsurfa.2014.07.049.

Pastorelli C., Formaro L., Ricca G., Severini F., 1999. Electrochemical behavior of the humic acid from leonardite. *Colloids Surf., B*, 13, 127–134. DOI: 10.1016/S0927-7765(99)00003-X.

Pierozynski B., Piotrowska G., 2018. Electrochemical degradation of phenol and resorcinol molecules through the dissolution of sacrificial anodes of macro-corrosion galvanic cells. *Water*, 10, 770. DOI: 10.3390/w10060770.

Ratnaweera H., Fettig J., 2015. State of the art of online monitoring and control of the coagulation process. *Water*, 7, 6574–6597. DOI: 10.3390/w7116574.

Sean Brossia C., 2014. 11 – The use of probes for detecting corrosion in underground pipelines, In: Orazem M.E. (Ed.), *Underground pipeline corrosion*. Woodhead Publishing, 286–303. DOI: 10.1533/9780857099266.2.286.

Sillanpää M., Matilainen A., 2015. Chapter 3 – NOM removal by coagulation, In: Sillanpää M. (Ed.), *Natural organic matter in water*. Butterworth-Heinemann, 55–80. DOI: 10.1016/B978-0-12-801503-2.00003-3.

Smallman R.E., Bishop R.J., 1999. Chapter 12 – Corrosion and surface engineering, In: Smallman R.E., Bishop R.J. (Eds.), Modern physical metallurgy and materials engineering (sixth edition). Butterworth-Heinemann, Oxford, 376–393. DOI: 10.1016/B978-075064564-5/50012-4.

Tatzber M., Stemmer M., Spiegel H., Katzlberger C., Haberhauer G., Mentler A., Gerzabek M.H., 2007. FTIR-spectroscopic characterization of humic acids and humin fractions obtained by advanced NaOH, $Na_4P_2O_7$, and Na_2CO_3 extraction procedures. *J. Plant Nutr. Soil Sci.*, 170, 522–529. DOI: 10.1002/jpln.200622082.

Ulu F., BarışçıS., Kobya M., Särkkä H., Sillanpää M., 2014. Removal of humic substances by electrocoagulation (EC) process and characterization of floc size growth mechanism under optimum conditions. *Sep. Purif. Technol.*, 133, 246–253. DOI: 10.1016/j.seppur.2014.07.003.

Wang D.S., Zhao Y.M., Yan M.Q., Chow C.W.K., 2013. Removal of DBP precursors in micro-polluted source waters: A comparative study on the enhanced coagulation behavior. *Sep. Purif. Technol.*, 118, 271–278. DOI: 10.1016/j.seppur.2013.06.038.

Xiao K., Dong C., Li X., Wang F., 2008. Corrosion products and formation mechanism during initial stage of atmospheric corrosion of carbon steel. *J. Iron Steel Res. Int.*, 15, 42–48. DOI: 10.1016/S1006-706X(08)60247-2.

Xiao K., Li Z., Song, J., Bai Z., Xue W., Wu J., Dong C., 2021. Effect of concentrations of Fe^{2+} and Fe^{3+} on the corrosion behavior of carbon steel in Cl^- and SO_4^{2-} aqueous environments. *Met. Mater. Int.*, 27, 2623–2633. DOI: 10.1007/s12540-019-00590-y.

Xiao Y.-H., Sara-Aho T., Hartikainen H., Vähätalo A.V., 2013. Contribution of ferric iron to light absorption by chromophoric dissolved organic matter. *Limnol. Oceanogr.*, 58, 653–662. DOI: 10.4319/lo.2013.58.2.0653.

Yousefi M., Nabizadeh R., Alimohammadi M., Mohammadi A.A., Mahvi A.H., 2019. Performance of granular ferric hydroxide process for removal of humic acid substances from aqueous solution based on experimental design and response surface methodology. *MethodsX*, 6, 35–42. DOI: 10.1016/j.mex.2018.12.010.

Zhu X., Chen X., Yang Z., Liu Y., Zhou Z., Ren Z., 2018. Investigating the influences of electrode material property on degradation behavior of organic wastewaters by iron-carbon micro-electrolysis. *Chem. Eng. J.*, 338, 46–54. DOI: 10.1016/j.cej.2017.12.091.